

A Conformal Wearable Antenna Based on Artificial Magnetic Conductor for GPS Applications

Shuqi Wang* and Yuqin Shi

Abstract—In order to improve the efficiency and safety of emergency rescue operations, a wearable circularly polarized (CP) antenna suitable for GPS applications has been designed. It adopts a coplanar waveguide (CPW)-fed structure, where the ground plane and radiation patch form an annular gap. The impedance bandwidth and axial ratio performance are enhanced by adjusting the amplitude and phase difference of the current distribution through two pairs of notches and open-circuit branches. When the single antenna is more than 20 millimeters away from the human body model, its CP radiation performance is acceptable, and the peak Specific Absorption Rate (SAR) also meets the required standards. To minimize the separation distance between the antenna and the human body, a 2×2 Artificial Magnetic Conductor (AMC) with in-phase reflection characteristics is integrated at the antenna's bottom as a reflector, which increases the antenna gain and reduces the SAR. Simulation and test results indicate that in the GPS L1 frequency band, the antenna achieves a gain greater than 7 dBi, an axial ratio less than 2 dB, a front-to-back ratio of 24 dB, and a peak SAR of 0.53 W/Kg, which is well below the standard limit of 1.6 W/Kg set by the Federal Communications Commission (FCC). Compared with other relevant antennas, this antenna features compact size, wide impedance bandwidth, and robust anti-interference capability, effectively improving the flexibility and compatibility of the wearable antenna, thereby meeting the demand for efficient and reliable positioning of rescuers.

1. INTRODUCTION

The accurate location information and navigation are crucial factors for improving the efficiency and safety of emergency rescue operations [1]. Conformable GPS wearable antennas can be integrated onto surfaces of different shapes and curvatures, and attached to clothing, helmets, belts, and other wearable equipment of trapped individuals or rescuers [2], which helps the command center to better understand their locations and make quick decisions, thereby enhancing efficiency and safety [3]. Considering that human activities may lead to antenna deformations and that human tissues exhibit complex electromagnetic properties influenced by external electromagnetic fields, it becomes crucial to address bending conformal behavior, frequency deviation, and polarization mismatch due to proximity to human tissues to minimize potential adverse effects of electromagnetic radiation on human health [4]. Therefore, the research significance lies in the safety and conformal design of wearable antennas for GPS applications.

In conventional wearable applications, several types of antennas have been proposed, including monopole antennas [5], microstrip patch antennas [6], planar inverted-F antennas [7], and button antennas [8]. Researchers have attempted to address the issues of antenna impedance mismatch and frequency shift caused by human tissues by adding a ground plane on the back of the antenna to reduce back radiation. For instance, Magdalena et al. introduced textile antennas using cotton and

Received 8 August 2023, Accepted 30 September 2023, Scheduled 17 October 2023

* Corresponding author: Shuqi Wang (wangshuqi@xust.edu.cn).

The authors are with the School of Communication and Information Engineering, Xi'an University of Science and Technology, Xi'an 710054, China.

silk substrates in the GPS L1 band, compared their performance, and analyzed their impact in free space and on-body conditions. Simulation and testing demonstrated that both antennas performed effectively at 1.575 GHz in a unidirectional radiation mod [9]. Poffelie et al. employed stacked patches and parasitic coupling to create a novel ultra-wideband textile antenna with a Fully-grounding (Fully-GD), achieving high on-body fidelity in the range of 3.18–11 GHz for ultra-wideband wireless body area network (WBAN) applications, but the antenna size is relatively large [10]. To further reduce electromagnetic radiation into the human body and lower the SAR, many researchers have introduced electromagnetic meta-surface structures in wearable antennas. For example, Yin et al. designed a WBAN wearable antenna for the ISM medical band using flexible polyimide material and loading a 2×2 AMC structure. This approach successfully reduced backward radiation, improved antenna gain, and resulted in an off-body gain of 7.47 dBi with a low SAR [11]. El Atrash et al. designed a low-profile, high-gain triangular slotted monopole dual-band antenna using the semi-flexible material Rogers 3850. The single antenna achieved favorable gain and SAR values at a distance of 15 millimeters from the human body model. To further improve performance, a 4×4 AMC array was loaded, reducing the distance between the antenna and the human body and achieving a lower profile [12]. In summary, various types of wearable antennas have been proposed to address performance issues caused by human tissues. The addition of ground planes and electromagnetic meta-surface structures, such as AMC structure, have been instrumental in reducing back radiation and improving antenna gain, thereby enhancing the overall performance of wearable antennas.

Most of the existing navigation antennas operate in right-handed circularly polarized (RHCP) mode, which reduces the antenna size and improves the radiation gain by using high dielectric constant ceramic antennas [13] or spiral antennas [14]. In recent years, wearable CP antennas have been extensively studied and explored by many researchers, who have employed different design methods and materials to improve the performance and applicability of the antenna. Joler and Boljkovac reported a sleeve-badge circularly polarized wearable fabric antenna with a gain of up to 5.04 dBi at 2.5 GHz, achieving an impedance bandwidth of 5.6% and a radiation efficiency of 55.3% [15]. Dierck et al. designed a wearable antenna covering GPS and satellite phone applications using flexible foam and polyimide materials, and improved the antenna gain by integrating a low noise amplifier chip at the bottom of the square patch [16]. Lee et al. proposed a wearable antenna integrated into a beret using a felt substrate and a conductive textile, with a cut corner square patch and four ring patches in metal short-circuited through holes to achieve dual indoor and outdoor GPS localization [17]. Pawase et al. designed a novel strip-fed, dual-frequency CP antenna, suitable for wearable GPS applications. It integrates a 2×2 Electromagnetic Band Gap (EBG) structure to reduce backward radiation and frequency detuning effects. The results indicate that this antenna achieves axial ratios of 2.23 dB and 2.39 dB at 1.13 GHz and 1.57 GHz [18].

These studies focus on optimizing the design and performance of wearable antennas to enhance the radiation efficiency and frequency characteristics. However, for wearable antennas with CP radiation characteristics, multiport feeding and coaxial feeding methods are slightly inadequate in terms of antenna fabrication and wearer comfort. In this paper, we propose a GPS conformal wearable antenna with a large impedance bandwidth and miniaturization to meet the requirements of emergency rescue positioning. By combining a single antenna with an AMC reflector, we analyze the antenna's reliability concerning bending stability in conformal configurations and safety in proximity to human tissue. The designed antenna exhibits high compatibility and flexibility to support positioning technology for emergency rescue operations.

2. DESIGN AND CONFIGURATION

A compact CPW-fed wearable CP antenna is proposed, in which the coupling of antenna and human body is effectively diminished by integrating the AMC structure. The antenna demonstrates an impressive impedance bandwidth of over 120 MHz, covering the L1 frequency band of GPS. Within this frequency range, the axial ratio remains below 2 dB; the front-to-back ratio exceeds 24 dB; and the gain surpasses 7 dBi.

2.1. CPW-Fed Slotted GPS Antenna Design

The conventional loop antenna exhibits a distribution of current that forms standing waves and radiates linearly polarized (LP) waves. However, CP radiation can be achieved through modifications to the loop antenna’s structure or by introducing perturbation elements. In this antenna, CP radiation is achieved by exciting a uniform traveling wave current on the loop and adjusting the amplitude and phase distribution of the current using changes in the patch structure or the addition of perturbation elements. The initial model of the antenna is that of an electrically large loop antenna, where the circumference of the loop is approximately equal to the free-space wavelength (λ_0) of the center frequency point. Consequently, the initial diameter of the radiating part of the loop is approximately $0.32\lambda_0$, and the maximum radiation direction corresponds to the axial direction of the loop.

Due to the favorable bandwidth characteristics and anti-interference capability of the CPW-fed antenna, this design is primarily based on a CPW-fed structure, as shown in Figure 1. The structure extends the ground plane part of the CPW towards the radiating patch direction, creating a circular gap inside. This extension of the ground plane increases the current distribution area and works together with the patch to achieve radiation functionality. The circular ring, comprising the gap and radiating patch, incorporates two pairs of notches and open-circuit branches. By adjusting the size of these notches, open-circuit branches, and the two vertical slits within the circular ring, the amplitude and phase difference of the electromagnetic wave can be controlled, enabling CP radiation. The antenna employs a polyimide substrate with a thickness of 1 mm and a relative permittivity of 3.5, with a size of $68.1 \times 65.6 \text{ mm}^2$ ($0.36\lambda_0 \times 0.35\lambda_0$). The CPW-fed antenna structure is simple and compact, significantly simplifying the manufacturing process and enhancing wearer comfort. The antenna’s performance is analyzed using electromagnetic simulation software, and the optimized structural dimensions are provided in Table 1.

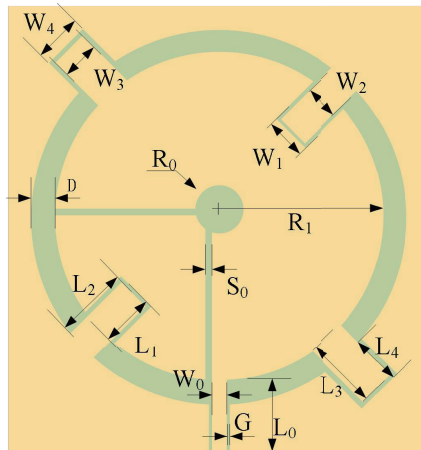


Figure 1. Structure of the proposed CPW-fed antenna.

Table 1. Dimensions of the proposed antenna in millimeters.

Parameter	R_0	R_1	D	W_0	L_0	S_0	G	W_1
value	10	25.8	4	1.7	9	1	0.4	5
Parameter	W_2	W_3	W_4	L_1	L_2	L_3	L_4	/
value	4	5	6	6	9	9	6	/

To preliminarily verify the radiation characteristics of the single antenna, Figure 2 presents the main simulation results of the antenna. From Figure 2(a), it can be observed that the S_{11} parameter of the antenna is below -10 dB in the range of 1.40 to 1.72 GHz, indicating an impressive impedance

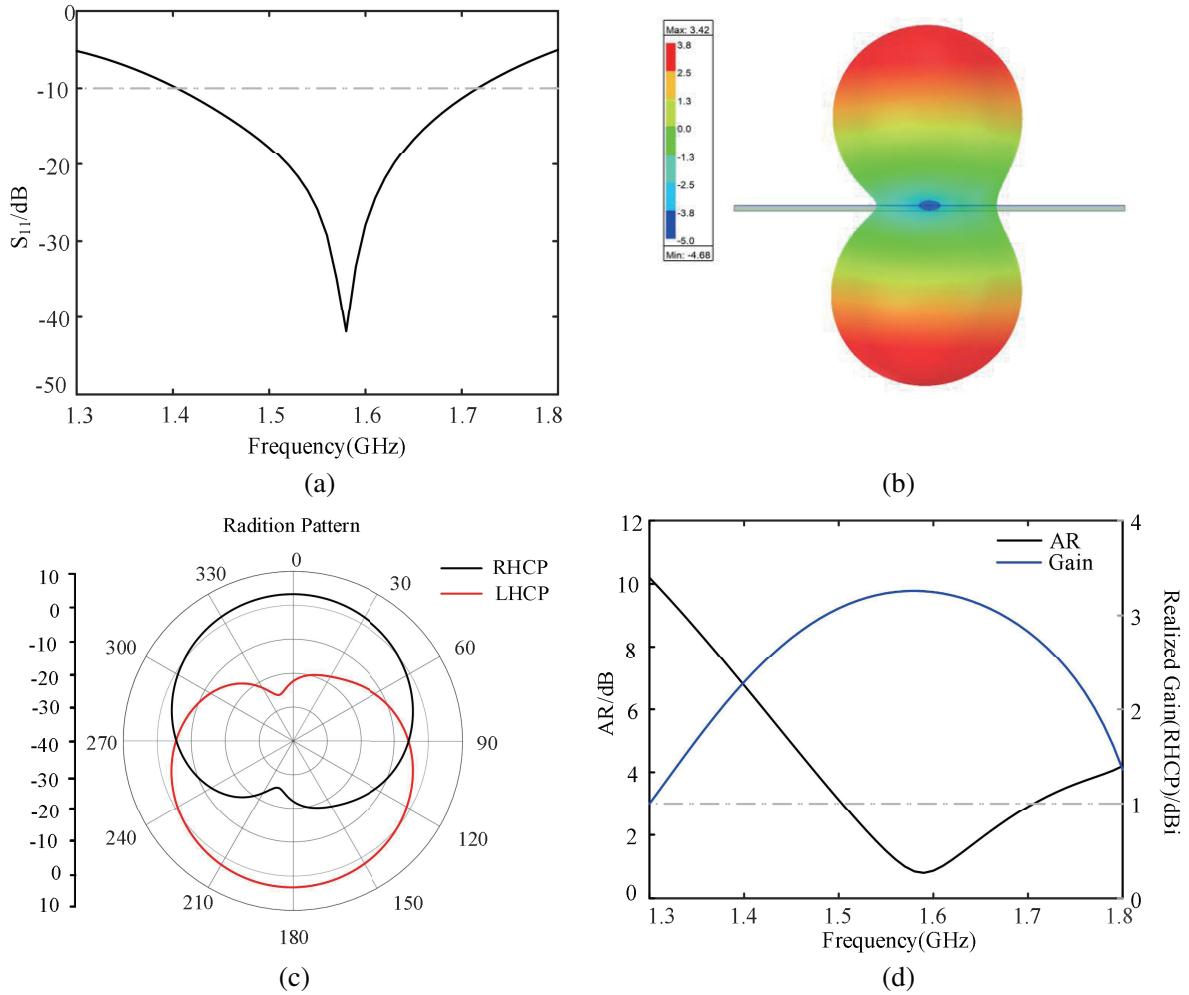


Figure 2. Simulated results of single CPW-fed antenna. (a) Simulated S_{11} of the CPW-fed antenna. (b) Simulated 3D radiation pattern of the CPW-fed antenna at 1.575 GHz. (c) Simulated RHCP and left-hand circular polarization (LHCP) radiation patterns in the xoz plane at plane. (d) Simulated Axial ratio and RHCP gain.

bandwidth broader than 20%. Moreover, at the operating frequency of 1.575 GHz, the S_{11} is below -38 dB, demonstrating a well-matched antenna. The radiation field distribution on both sides of the dielectric substrate is relatively symmetric, as depicted in Figure 2(b), with a front-to-back ratio of approximately 0 dB, consistent with the bidirectional radiation propagation characteristics of the CPW antenna. The radiation pattern in the xoz plane, presented in Figure 2(c), reveals that the antenna emits RHCP waves in the upper half-space along the z -axis, with a half-power beamwidth approximately $\pm 50^\circ$. Figure 2(d) illustrates the axial ratio and gain, indicating that within the 1575 ± 30 MHz range, the antenna's axial ratio remains below 1.5 dB, and the RHCP gain exceeds 3.2 dBi, with a radiation efficiency over 97%. These results demonstrate the antenna's excellent radiation characteristics.

2.2. Design of AMC Structure

To reduce the coupling effect between the antenna and human body tissues and minimize radiation towards the body, a 2×2 square ring AMC structure was designed as a reflector. It operates based on the principle of in-phase and out-of-phase reflection of the AMC structure, as depicted in Figure 3(a), with added slots to increase the effective current path and reduce the antenna size. The AMC reflector was fabricated using a 1.5 mm-thick polyimide substrate. Incorporating the AMC reflector leads to

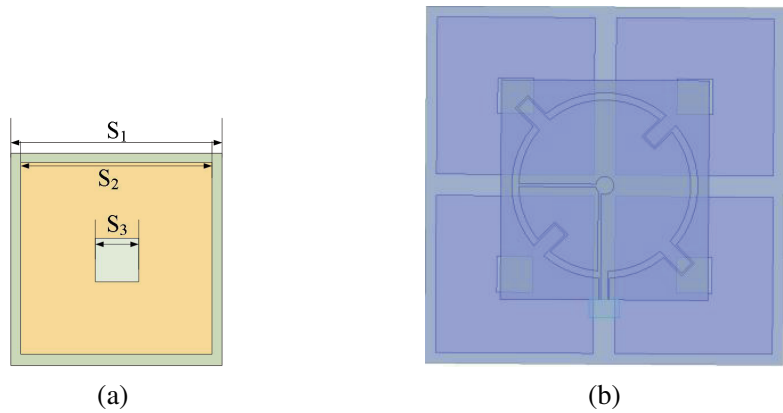


Figure 3. CPW-fed Antenna Loaded with AMC Array. (a) Design of the AMC unit. (b) AMC structure loaded at the bottom of the antenna.

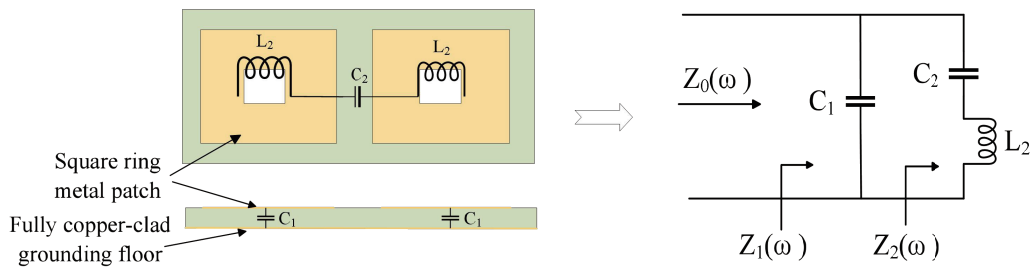


Figure 4. Equivalent circuit of the square ring AMC structure.

improved gain and Specific Absorption Rate (SAR) values.

The equivalent circuit of the AMC structure is shown in Figure 4, and its surface impedance can be expressed as:

$$Z_0(\omega) = Z_1 // Z_2 = \frac{j(1 - \omega^2 C_1 L_2)}{\omega(C_1 C_2 L_2 \omega^2 - C_1 - C_2)}$$

The resonant frequency of the AMC can be calculated from the above equation as:

$$f_0 = \frac{1}{2\pi} \sqrt{\frac{C_1 + C_2}{C_1 C_2 L_2}}$$

where C_1 , C_2 , and L_2 represent the equivalent capacitance between the patch and grounding plate, the equivalent capacitance between the adjacent periodic unit patches, and the equivalent inductance of the square ring-shaped metal patch, respectively. To achieve the in-phase reflection bandwidth required for the operating frequency point, the corresponding equivalent capacitance, and equivalent inductance can be changed by adjusting the inner and outer edge lengths S_2 and S_3 of the square ring and the thickness of the dielectric plate.

2.3. Loaded AMC Array of Wearable Antennas

Due to the electromagnetic coupling between the single antenna and the AMC structure, as well as the assumption of an ideal plane wave and the use of Floquet ports in the AMC design process, it becomes necessary to optimize and adjust the original antenna dimensions, the AMC structure, and the spacing between them. The final model structure, as depicted in Figure 3(b), consists of antenna dimensions of $61.5 \times 58 \text{ mm}^2$ and AMC reflector dimensions of $100 \times 100 \text{ mm}^2$, separated by 7 mm foam. The optimized dimensions are presented in Table 2.

Table 2. Adjusted dimensions of the final antenna in millimeters.

Parameter	R_0	R_1	D	W_0	L_0	S_0	G	W_1	W_2
Value	2.5	24	2	2	8	0.8	0.4	5	4
Parameter	W_3	W_4	L_1	L_2	L_3	L_4	S_1	S_2	S_3
Value	4	5	7	8.5	8.5	7	50	44	10

The radiation performances of the antenna with and without the loaded AMC structure are compared in Figure 5. Simulation results indicate that even after loading the AMC structure, the antenna retains its RHCP characteristics, boasting a -10 dB impedance bandwidth of 120 MHz ($1.52 \sim 1.64$ GHz) and an axial ratio of less than 3 dB within the 1575 ± 10 MHz range, while achieving a gain of more than 6.8 dBi. This configuration leads to a hemispherical radiation pattern, and the front-to-back ratio (FBR) exceeds 24 dB, denoting directional radiation. Despite a noticeable reduction in impedance bandwidth and axial ratio bandwidth compared to the antenna without the AMC structure, the addition of the AMC reflector significantly increases gain and FBR while modifying the original

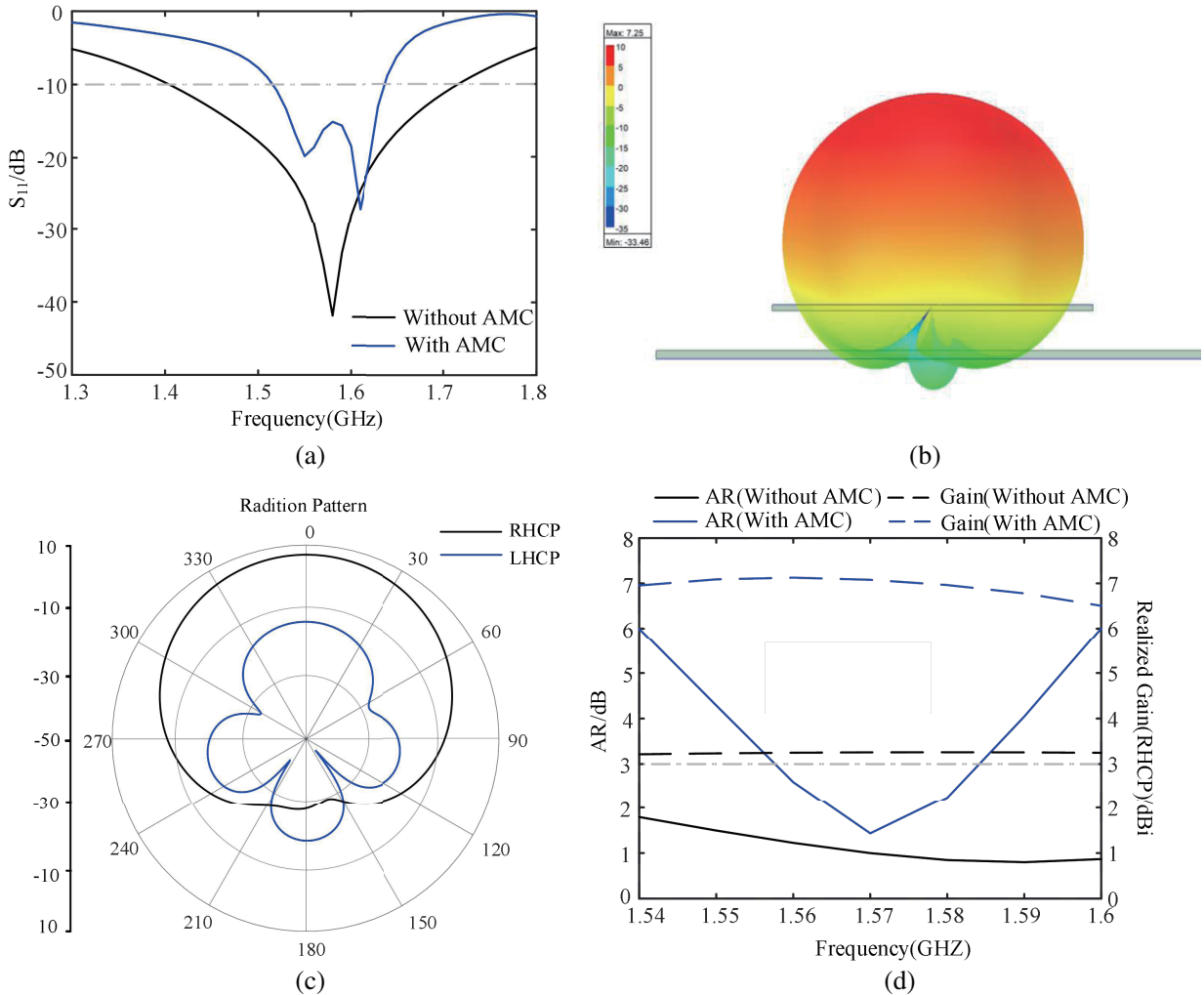


Figure 5. Comparison of results with and without AMC reflector loading. (a) Simulated S_{11} comparison plot. (b) 3D radiation pattern for loaded AMC reflector plate. (c) XOZ surface radiation pattern with loaded AMC reflector. (d) Comparison of axial ratio and actual gain with RHCP.

bidirectional radiation characteristics. Preliminary simulation results suggest that the antenna system meets the operational requirements of the GPS L1 band.

3. RELIABILITY ANALYSIS OF WEARABLE ANTENNA

The reliability of wearable antennas pertains to the ability of the antenna system or its components to function consistently and dependably under specific conditions, fulfilling their intended functions. In this design, our main focus is to analyze the bending stability under various curvature radii and the safety aspects in close proximity to human body tissues.

3.1. Bending Stability Analysis of Wearable Antennas

Due to the requirement of achieving conformal integration with the human body surface, wearable antennas face challenges, such as polarization mismatch caused by the movement of the antenna with the human body. Therefore, conducting research on wearable antennas with good bending stability is crucial. As depicted in Figure 6, this study employs cylindrical models with curvature radii of $R_w = 40$ mm, 80 mm, and 160 mm to approximate the human upper arm, leg, and chest-back regions, respectively, in order to analyze the radiation characteristics of the wearable antenna under bending conformal conditions. The analysis examines the effect of different radii of curvature along the x -axis on the antenna's performance in free space.

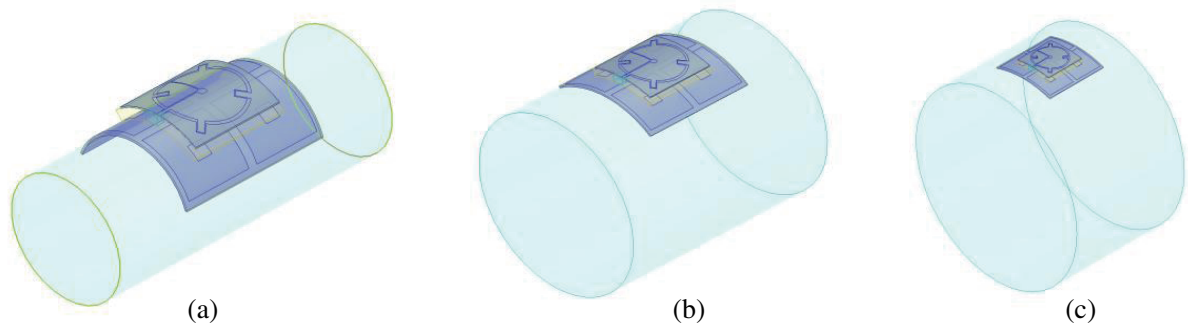


Figure 6. Bending conformal model of the antenna with AMC structure. (a) $R_w = 40$ mm (b) $R_w = 80$ mm (c) $R_w = 160$ mm.

To investigate the radiation characteristics of the designed antenna under bending conformal conditions, simulation analyses were performed separately for two scenarios: the single antenna system and the antenna with an attached AMC array.

Figure 7(a) displays the S_{11} simulation results of the single antenna under varying bending radius. The overall resonant frequency shifts slightly to the left by about 20 MHz, mainly due to the increased effective path of the current after bending. Moreover, a smaller bend radius leads to a slight decrease in impedance bandwidth, resulting in poorer impedance matching. Figure 7(b) illustrates the impact of bend radius on the axial ratio and gain. As the bending radius decreases, the axial ratio bandwidth also decreases, leading to lower RHCP gain. These losses fall within an acceptable range and fully satisfy the requirements for navigation in the GPS L1 frequency band. In summary, the simulation results demonstrate that despite minor changes in resonant frequency, impedance bandwidth, axial ratio, and gain under different bending conditions, the antenna performance remains suitable for GPS L1 navigation applications.

The simulation results of the antenna with the AMC structure under different degrees of bending are presented in Figure 8 and Table 3. In the bending scenario, the addition of the reflector caused significant shifts in the resonant frequency of the antenna, particularly at $R_w = 40$ mm, where the axial ratio bandwidth and gain loss were considerable, resulting in an FBR of only 14 dB compared to the single antenna model. However, as the bending radius increased, the axial ratio bandwidth and

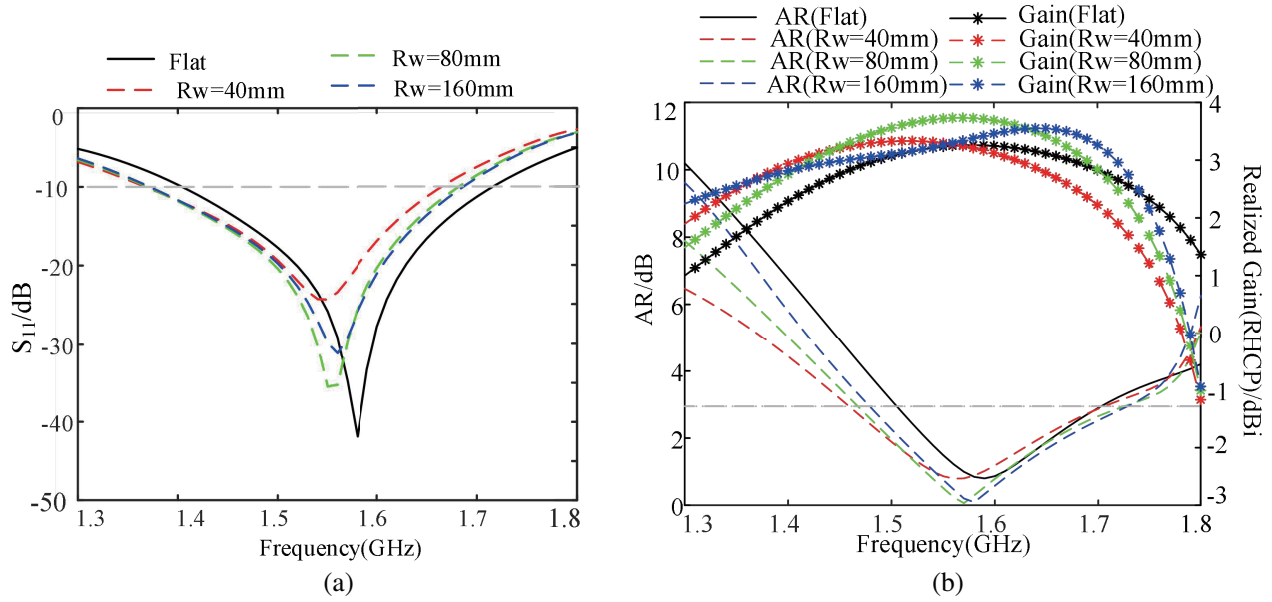


Figure 7. The effect of different degrees of bending on the main parameters of the antenna in the case of a single antenna. (a) The effect of different bending radius Rw on S_{11} . (b) The effect of different bending radius Rw on axial ratio and gain.

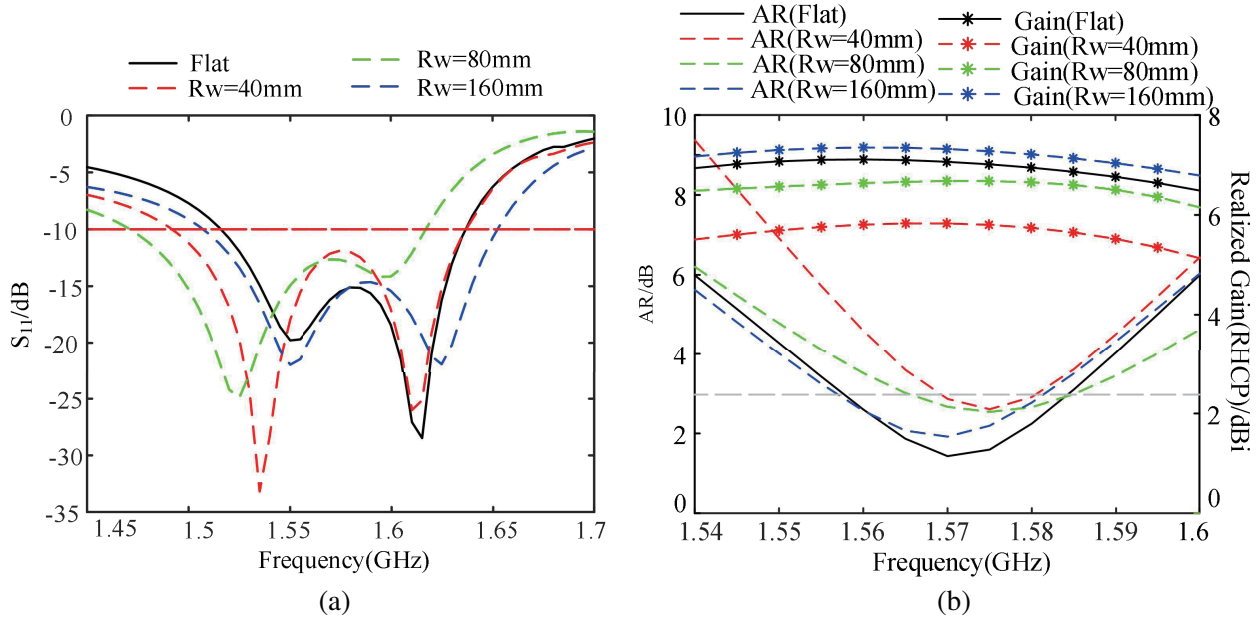


Figure 8. Bending conformal simulation of the antenna with the loaded AMC structure. (a) Comparison of simulated S_{11} . (b) Comparison of simulated axial ratio and gain.

gain of the antenna showed relative improvements, leading to increased FBR and radiation efficiency. Remarkably, at $Rw = 160$ mm, the radiation performance of the antenna surpassed that of the flat state, primarily due to the bending conformal configuration, which altered the electromagnetic field distribution and radiation characteristics, resulting in enhanced gain and directivity. Consequently, the antenna exhibited superior radiation performance in the bending state. Under different bending conditions, the radiation efficiency remained above 80%, and the radiation characteristics proved stable, effectively fulfilling the requirements for positioning work in the GPS L1 frequency band.

Table 3. Comparison of front-to-back ratio and radiation efficiency under bending conformal conditions.

	Flat	$Rw = 40$ mm	$Rw = 80$ mm	$Rw = 160$ mm
FBR	24	14	16	18
Radiation efficiency (η)	85%	81%	87%	87%

3.2. Safety Analysis of Wearable Antennas

SAR refers to the rate at which electromagnetic radiation energy is absorbed or dissipated per unit mass of a substance in a given time. For wearable antennas, SAR stands as a crucial parameter impacting human safety. Its formula for calculation can be expressed as follows:

$$\text{SAR} = \frac{d}{dt} \left(\frac{dW}{dm} \right) = \frac{d}{dt} \left(\frac{dW}{\rho dV} \right) = \frac{\sigma E^2}{\rho}$$

where σ signifies the conductivity of human tissue in S/m, ρ the mass density of the tissue in kg/m^3 , and E the electric field strength in the tissue in V/m. The FCC imposes a limit that the average SAR value for 1 g of human tissue should not exceed 1.6 W/kg.

In this study, we generate an electromagnetic tissue model of the human body measuring $150 \times 150 \times 33 \text{ mm}^3$ using simulation software. The model encompasses three layers of human tissue: a 2 mm-thick skin layer, an 8 mm-thick fat layer, and a 23 mm-thick muscle layer. This particular model finds widespread application in the analysis of wearable devices [19]. The electromagnetic characteristic parameters of each tissue layer at 1.575 GHz are detailed in Table 4.

Table 4. Electromagnetic parameters of major human tissues at 1.575 GHz [20].

Human Tissue	Conductivity (S/m)	Relative permittivity	Density (kg/m^3)
Skin	1.0991	53.92	1001
Fat	0.0705	5.3747	900
Muscle	1.2244	53.856	1006

Based on benchmark testing, an input power of 100 mW has been opted for the purpose of conducting a comparative analysis regarding the safety aspects of this antenna. As shown in Figure 9(a), when the single antenna is 1 mm away from the human body tissue, the peak value of SAR corresponding to 1 g of human body tissue is 4.97 W/kg. This measurement falls short of meeting the electromagnetic radiation protection standards outlined by the FCC. Furthermore, due to the interplay of coupling between the antenna and the human body, the antenna demonstrates suboptimal radiative performance, resulting in a mere 5.5% radiation efficiency. In contrast, Figure 9(b) demonstrates that by increasing the separation distance between the antenna and the human body, the antenna's performance aligns more closely with the design requirements. Notably, the antenna's performance meets the desired criteria when the distance from the human body model exceeds 20 mm. This improved performance is characterized by an impedance bandwidth of 310 MHz (1.35 ~ 1.66 GHz), an axial ratio bandwidth of 140 MHz (1.44 ~ 1.58 GHz), a peak gain of 1.6 dBi, and a lower SAR value of approximately 0.93 W/kg. The latter measurement comfortably falls below the electromagnetic radiation protection standard stipulated by the FCC. Additionally, the enhancement in antenna radiation efficiency is substantial, reaching 31%.

In Figure 9(c), the antenna equipped with an AMC reflector is positioned 1 mm above a human tissue model. The simulated peak value of SAR is recorded at 0.53 W/kg. Remarkably, this value is

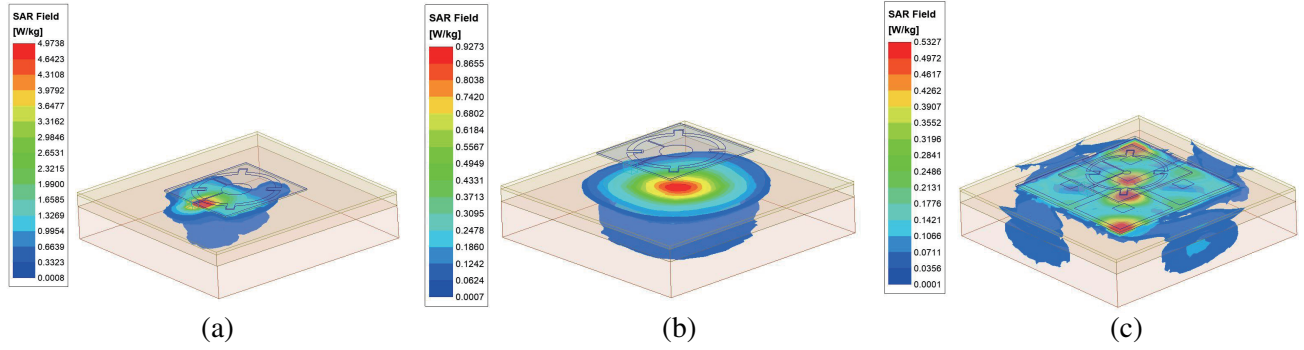


Figure 9. SAR Analysis of the Antenna Model. (a) Distance between the single antenna and human tissue model is 1 millimeter. (b) Distance between the single antenna and human tissue model is 20 millimeters. (c) Distance between the antenna with loaded AMC reflector and human tissue model is 1 millimeter.

significantly lower than the SAR peak observed without the AMC reflector at the same 1 mm distance from the human tissue. The reduction is a substantial 89%, effectively placing it well below the FCC’s standard of 1.6 W/kg. At this configuration, the radiation efficiency improves to 85%. Table 5 provides a succinct comparative analysis of the SAR values and radiation efficiency of the single antenna model and the antenna integrated with the AMC structure across varying conditions. It is evident that the inclusion of the AMC reflector effectively severs the antenna’s connection with the human body, resulting in a decreased absorption of radiation energy by the human body. This consequently minimizes the influence of human body electromagnetic traits on antenna performance. Consequently, the antenna aligns with the electromagnetic radiation protection standard stipulated by the FCC.

Table 5. SAR values and antenna radiation efficiency of the antenna under different conditions.

	Distance from human tissue model (mm)	Peak SAR (W/Kg)	Radiation efficiency
Single Antenna Model	1 mm	4.97	5.5%
	20 mm	0.93	31%
Loaded AMC structure	1 mm	0.53	85%

4. FABRICATION AND TESTING OF THE ANTENNA PROTOTYPE

To validate the initial design and simulation efforts, and to gauge the viability and effectiveness of the proposed antenna, the antenna was physically constructed and subjected to testing using the simulation model as a basis. The objective of the testing was to assess the antenna’s return loss, axial ratio, gain, and radiation pattern, subsequently comparing and corroborating the findings with the simulated outcomes. In Figure 10, the tangible prototype of the CPW-fed circularly polarized wearable antenna is illustrated utilizing the AMC structure, along with the test setting.

The physical antenna underwent testing utilizing an Agilent E8362C Vector Network Analyzer within a microwave anechoic chamber. The outcomes of the antenna are displayed in Figure 11 across three distinct scenarios: simulation in free space, actual testing in free space, and testing in proximity to a human body. In Figure 11(a), the substantial congruence between the measured S_{11} and simulation results of the antenna in free space is illustrated. The impedance bandwidth spans from 1.53 GHz to 1.64 GHz, with the S_{11} value registering at -18 dB at 1.575 GHz, thus achieving a commendable match. However, when the antenna is close to a human body, the dielectric properties of the human tissue alter the equivalent capacitance and inductance of antenna, causing a shift in the resonant frequency to lower

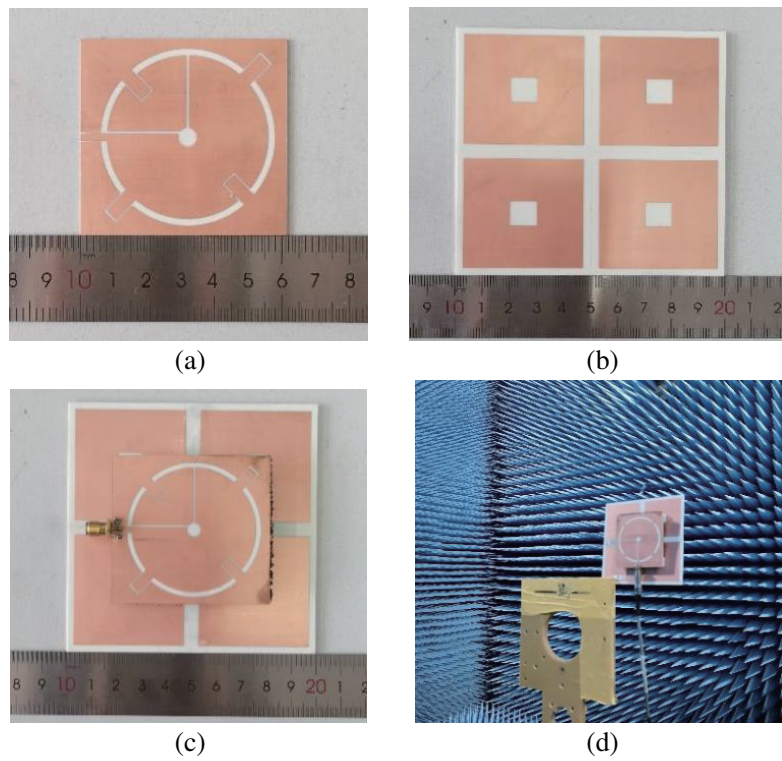


Figure 10. Physical Antenna prototype and its test environment. (a) Antenna section. (b) AMC reflector section. (c) Antenna loaded AMC reflector. (d) Far-field test environment.

Table 6. Performance comparison with other antennas.

Ref.	Reflection Mode	Dimension (mm ²)	Impedance BW (MHz)	Operating range (LP/CP)	Gain (dBi)
[1]	NO	33 × 220 (0.17λ ₀ × 1.16λ ₀)	90/370 (5.7%, 15.1%)	ISM2.45 (LP) /GPS L1 (LP)	4.8/6.6
[3]	NO	255.2 × 36.7 (0.34λ ₀ × 0.05λ ₀)	/	EPIRB (LP) /GPS L1 (LP)	/
[9]	Fully-GD	100 × 110 (0.53λ ₀ × 0.58λ ₀)	82 (5.2%)	GPS L1 (LP)	4.011
[10]	Fully-GD	80 × 61 (0.85λ ₀ × 0.65λ ₀)	7820 (114.2%)	UWB 3.1 ~ 10.6 (LP)	1 ~ 7
[11]	2 × 2 AMC Array	66.8 × 66.8 (0.54λ ₀ × 0.54λ ₀)	83.5 (3.4%)	ISM 2.4 (LP)	7.48
[12]	4 × 4 AMC Array	86 × 86 (1.00λ ₀ × 1.00λ ₀)	200/434 (5.7%/7.4%)	Wimax 3.5 (LP) /ISM 5.8 (LP)	9.4/6.6
[15]	Fully-GD	57 × 50 (0.46λ ₀ × 0.40λ ₀)	137 (5.6%)	ISM 2.4 (CP)	5.04
This Paper	2 × 2 AMC Array	100 × 100 (0.53λ ₀ × 0.53λ ₀)	120 (7.6%)	GPS L1 (CP)	7.15

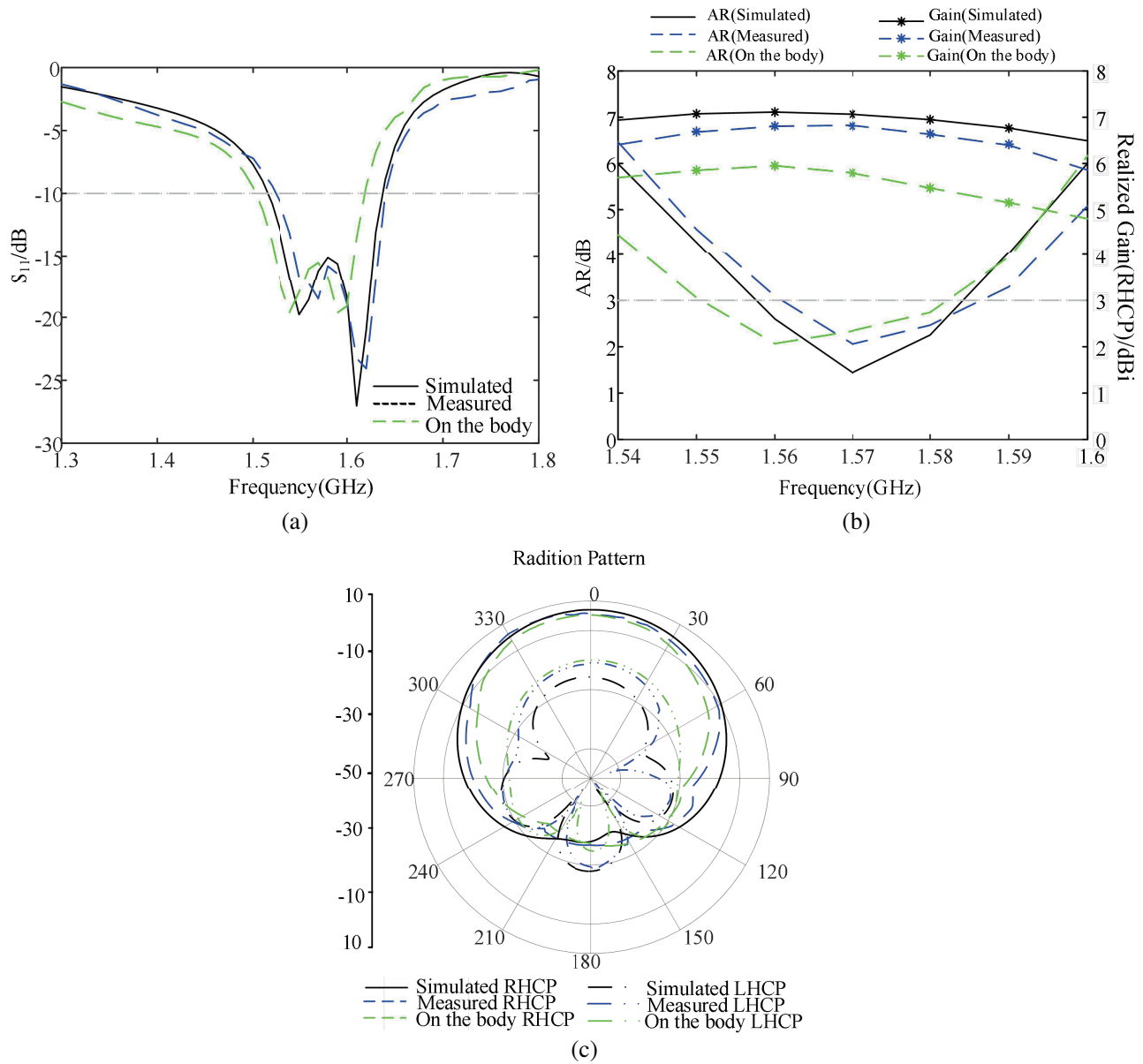


Figure 11. Antenna test results. (a) Plot of S_{11} results. (b) Plot of axial ratio and gain. (c) Radiation pattern of XOZ plane.

frequencies. Consequently, the frequency point optimal for the axial ratio and gain experiences a slight leftward shift, as depicted in Figure 11(b). Nonetheless, even under free-space conditions, the measured gain with right circular polarization within the range of 1.575 ± 10 MHz still attains 7 dBi, accompanied by an axial ratio below 3 dB. Notably, the antenna maintains coverage of the GPS L1 frequency band. Furthermore, Figure 11(c) affirms the retention of favorable directional radiation characteristics in the measured outcomes, with the antenna demonstrating a hemispherical radiation pattern in the xoz plane. The front-to-back ratio exceeds 20 dB, aligning closely with the simulation findings.

Through a comparison of simulation and actual measurement results, minor disparities were discerned in the overall test outcomes as opposed to the frequency points simulated. These deviations could be ascribed to factors encompassing material properties during the practical manufacturing process, processing inaccuracies, and losses in connectors. Notwithstanding these marginal variations, the comprehensive measured outcomes closely mirror the simulation results, thereby affirming the

viability of the design methodology.

Table 6 is provided for the purpose of comparing the key performance metrics and parameters with those found in other pertinent references. Notably, it becomes evident that the newly developed antenna boasts the most compact form factor, all the while possessing advantageous characteristics in terms of impedance bandwidth. This enhancement significantly augments the versatility and suitability of the conformal wearable antenna. Furthermore, within the GPS operating frequency band, it demonstrates notably superior circular polarization performance, effectively bolstering its resistance to the effects of multipath interference. With its remarkable compatibility, this antenna is poised to deliver steadfast and dependable GPS signal reception and positioning capabilities, especially in critical scenarios demanding emergency rescue missions.

5. CONCLUSION

A novel conformal wearable antenna designed for the GPS L1 frequency band incorporates a 2×2 AMC reflector at its base to mitigate radiation directed toward the body. This antenna is characterized by its straightforward yet compact structure, wider impedance bandwidth, increased gain, and enhanced anti-interference capabilities. Analysis of the antenna's radiation performance under bending conformal conditions and its SAR value in proximity to the body affirms the proposed antenna's reliability. Notably, it achieves an impedance bandwidth of 120 MHz and an axial ratio bandwidth of 27 MHz. The integration of the reflector yields exceptional radiation characteristics within the GPS L1 frequency band, featuring a peak gain of 7.15 dBi, an FBR of 24 dB, and a minimal SAR peak of 0.53 W/kg. The design affirms the CPW-fed circular slot antenna's ability to achieve a wide impedance bandwidth and circular polarization. Additionally, it underscores the efficacy of an AMC structure in minimizing antenna radiation hazards. Furthermore, the design underwent physical fabrication and testing based on simulation, with test results largely aligning with the simulated outcomes. This alignment holds significant implications for the future research and development of emergency rescue and wearable positioning services.

ACKNOWLEDGMENT

This work was supported by the National Natural Science Foundation of China [61901357].

REFERENCES

1. Das, S., H. Islam, and T. Bose, "Compact low-profile body worn and wrist worn lightweight antenna for ISM and GPS band navigation and medical applications," *Microwave and Optical Technology Letters*, Vol. 60, No. 9, 2122–2127, 2018.
2. Ali, U., S. Ullah, B. Kamal, et al., "Design, analysis and applications of wearable antennas: A review," *IEEE Access*, 2023.
3. Alkhamis, R., J. Wigle, and H. Song, "Global positioning system and distress signal frequency wrist wearable dual-band antenna," *Microwave and Optical Technology Letters*, Vol. 59, No. 8, 2057–2064, 2017.
4. Chaouche, Y. B., M. Nedil, I. B. Mabrouk, et al., "A wearable circularly polarized antenna backed by AMC reflector for WBAN communications," *IEEE Access*, Vol. 10, 12838–12852, 2022.
5. Chen, P., D. Wang, and Z. Gan, "Flexible and small textile antenna for UWB wireless body area network," *Micromachines*, Vol. 14, No. 4, 718, 2023.
6. Li, H., J. Du, X. X. Yang, et al., "Low-profile all-textile multiband microstrip circular patch antenna for WBAN applications," *IEEE Antennas and Wireless Propagation Letters*, Vol. 21, No. 4, 779–783, 2022.
7. Gao, G. P., C. Yang, B. Hu, et al., "A wide-bandwidth wearable all-textile PIFA with dual resonance modes for 5 GHz WLAN applications," *IEEE Transactions on Antennas and Propagation*, Vol. 67, No. 6, 4206–4211, 2019.

8. Banafaa, M. K., M. H. Jamaluddin, S. H. Dahlan, et al., "Miniature dual band button antenna using cylindrical dielectric resonator antenna for on/off body communication devices," *The Applied Computational Electromagnetics Society Journal (ACES)*, 479–485, 2021.
9. Magdalena, Y., R. Anwar, Y. Wahyu, et al., "Performance comparison of cotton and silk substrates on 1.575 GHz frequency textile antenna," *Elektronika Ir Elektrotehnika*, Vol. 27, No. 5, 26–33, 2021.
10. Poffelie, L. A. Y., P. J. Soh, S. Yan, et al., "A high-fidelity all-textile UWB antenna with low back radiation for off-body WBAN applications," *IEEE Transactions on Antennas and Propagation*, Vol. 64, No. 2, 757–760, 2015.
11. Yin, B., J. Gu, X. Feng, et al., "A low SAR value wearable antenna for wireless body area network based on AMC structure," *Progress In Electromagnetics Research C*, Vol. 95, 119–129, 2019.
12. El Atrash, M., M. A. Abdalla, and H. M. Elhennawy, "A wearable dual-band low profile high gain low SAR antenna AMC-backed for WBAN applications," *IEEE Transactions on Antennas and Propagation*, Vol. 67, No. 10, 6378–6388, 2019.
13. Park, M., W. Lee, and T. Son, "Composite GPS patch antenna for the AR bandwidth enhancement," *International Journal of Antennas and Propagation*, Vol. 2016, 2016.
14. Guo, L., P. Zhang, F. Zeng, et al., "A novel four-arm planar spiral antenna for GNSS application," *IEEE Access*, Vol. 9, 168899–168906, 2021.
15. Joler, M. and M. Boljkovac, "A sleeve-badge circularly polarized textile antenna," *IEEE Transactions on Antennas and Propagation*, Vol. 66, No. 3, 1576–1579, 2018.
16. Dierck, A., H. Rogier, and F. Declercq, "A wearable active antenna for global positioning system and satellite phone," *IEEE Transactions on Antennas and Propagation*, Vol. 61, No. 2, 532–538, 2012.
17. Lee, H., J. Tak, and J. Choi, "Wearable antenna integrated into military berets for indoor/outdoor positioning system," *IEEE Antennas and Wireless Propagation Letters*, Vol. 16: 1919–1922, 2017.
18. Pawase, T., A. Malhotra, and A. Mahajan, "Compact hybrid EBG microstrip antenna for wearable applications," *Frequenz*, 2023.
19. Chen, Y. S. and T. Y. Ku, "A low-profile wearable antenna using a miniature high impedance surface for smartwatch applications," *IEEE Antennas and Wireless Propagation Letters*, Vol. 15, 1144–1147, 2015.
20. Sasaki, K., E. Porter, E. A. Rashed, et al., "Measurement and image-based estimation of dielectric properties of biological tissues — past, present, and future," *Physics in Medicine & Biology*, Vol. 67, No. 14, 14TR01, 2022.